Lab on a Chip

Cite this: DOI: 10.1039/c1lc20257j

www.rsc.org/loc

PAPER

High fidelity neuronal networks formed by plasma masking with a bilayer membrane: analysis of neurodegenerative and neuroprotective processes†

Heike Hardelauf,[a] Julia Sisnaiske,[b] Amir Ali Taghipour-Anvari,[c] Peter Jacob,[a] Evelyn Drabiniok,[c] Ulrich Marggraf,[ac] Jean-Philippe Frimat,[d] Jan G. Hengstler,[b] Andreas Neyer,[c] Christoph van Thriel[b] and Jonathan West*[a]

Received 25th March 2011, Accepted 8th June 2011
DOI: 10.1039/c1lc20257j

Spatially defined neuronal networks have great potential to be used in a wide spectrum of neurobiology assays. We present an original technique for the precise and reproducible formation of neuronal networks. A PDMS membrane comprising through-holes aligned with interconnecting microchannels was used during oxygen plasma etching to dry mask a protein rejecting poly(ethylene glycol) (PEG) adlayer. Patterns were faithfully replicated to produce an oxidized interconnected array pattern which supported protein adsorption. Differentiated human SH-SY5Y neuron-like cells adhered to the array nodes with the micron-scale interconnecting tracks guiding neurite outgrowth to produce neuronal connections and establish a network. A 2.0 μm track width was optimal for high-level network formation and node compliance. These spatially standardized neuronal networks were used to analyse the dynamics of acrylamide-induced neurite degeneration and the protective effects of co-treatment with calpeptin or brain derived neurotrophic factor (BDNF).

Introduction

Cellular adhesion patterns have become increasingly recognized as valuable tools for fundamental research into the effect of dimensional and geometric parameters on the cytoskeletal architecture and downstream responses.[1] Micropatterning can be applied with equal effect to industrial applications such as tissue engineering,[2] as well as drug discovery[3–6] and toxicology screening.[4,7,8] Here the goal is to preserve authentic cell structure and behaviour, with the spatial ordering of the cultures used to define the tissue dimensions, geometries and associated diffusion gradients. Ordering the culture within an array format also has the telling advantage of providing a display for rapid and high content analysis.[7,9,10]

The striking form–function relations of the brain and the nervous system have inspired many researchers to replicate engineered analogs in the form of spatially defined neuronal networks. Seminal work by Kleinfeld *et al.* involved using this approach to investigate signal propagation through a prescribed neuronal network.[11] In recent years such patterns have been aligned with microelectrode arrays to provide electronically addressable interfaces at the nodes within the network.[12–16] Neurite outgrowth and connectivity are useful neuro-developmental indicators in themselves. We have spatially standardized the process within a hexagonally patterned array for rapid, reproducible and quantitative neurotoxicology screening.[7]

There is a huge repertoire of micropatterning techniques from which to choose. In the simplest form hydrophilic–hydrophobic surface contrasts can be prepared by a number of routes including deep UV photochemical patterning[17,18] or by masking with photoresists[19,20] or with stencils[21,22] during plasma-based oxidative patterning of hydrophobic backgrounds. Similarly, aminated silane coatings assist cell adhesion and can be photolithographically patterned along with hydrophobic silanes to confine the cellular adhesion microenvironment.[11,19,23]

Physicochemical surface patterns are sufficient for patterning cell lines. However, when working with primary and stem cell cultures, proteins are necessary for adhesion, function and maintenance of the differentiated state. Moreover, the use of proteins, typically constituents of the extracellular matrix, provides a more relevant context for mimicking the *in vivo* adhesive environment. However, the solvents required for photoresist processing are not sufficiently biocompatible for most proteins.[24,25] Soft lithography, notably in the form of microcontact printing (μCP), sidesteps the use of solvents with instead PDMS replica moulds being used to transfer patterns of

[a]*Leibniz Institut für Analytische Wissenschaften-ISAS-e.V., Otto-Hahn-Str. 6b, 44227 Dortmund, Germany. E-mail: west@isas.de*
[b]*Leibniz Research Centre for Working Environment and Human Factors at the University of Dortmund (IfADo), Ardeystr. 67, 44139 Dortmund, Germany*
[c]*Micro Structure Technology Laboratory, Faculty of Electrical Engineering, TU Dortmund, 44221 Dortmund, Germany*
[d]*BIOS–Lab on a Chip Group, MESA+, University of Twente, Enschede, The Netherlands*

† Electronic supplementary information (ESI) available. See DOI: 10.1039/c1lc20257j

biologically active proteins.[26,27] The elastomeric character of PDMS enables conformal contact with substrates for micron-scale patterning outside the clean room and importantly places a simple and inexpensive replication technology in the hands of the biologists.[28,29] For these reasons protein μCP has earned widespread popularity, with a number of examples demonstrating the ability to pattern neurons (*e.g.* by Vogt *et al.*).[30]

Patterning neuronal networks presents a unique challenge, with the need for micron-scale protein tracks which must equally support neurite outgrowth and prevent the adhesion of cell bodies. While often overlooked, across chip, chip-to-chip and batch-to-batch reproducibility is another essential aspect for undertaking experiments with confidence. As with all patterning techniques, protein μCP has limitations, including difficulties with producing homogeneous prints, which is especially hampered at the pattern edge.[31,32] In addition, the deformable character of PDMS prohibits the use of small stamp features separated by comparatively large distances (*i.e.* those required for patterning neuronal networks) which are prone to collapse and foul regions otherwise intended to resist cell adhesion.[16,32,33] This prevents the reproducible fabrication of neuronal arrays with micron-scale interconnecting tracks. Although more rigid stamp materials could be used, this is at the expense of conformal contact which further reduces the pattern uniformity.

In place of protein printing, materials with different affinities for protein adsorption can be combined and used to pattern cells. Poly(ethylene glycol) (PEG) surfaces are famed for their ability to resist protein adsorption and thus cell adhesion.[34,35] Contact printing can be used to pattern the grafted copolymer of poly-L-lysine with PEG (PLL-*g*-PEG) on culture surfaces, where proteins self assemble on the uncoated regions to support cell adhesion.[36] As with protein printing, across pattern reproducibility is brought into question and instead photoresist-based processing of PEG layers can be used.[32,37,38] Alternatively, deep UV (185 nm) photolithography can be used for across wafer patterning by photodegradation.[39,40] For micron-scale patterning contact masking is required, a feature which greatly reduces the lifespan of the costly quartz masks necessary for UV transmission. These standard photolithography methods demand clean room operation, which removes the freedom of replication from the end user.[29,31,39]

In our previous work we developed a thin film PDMS printing technique for obtaining hydrophilic–hydrophobic surface contrasts. Array patterns were suitable for undertaking the network formation assay (NFA) with neuron-like cell lines.[7] To extend the NFA to other neuron types, including primaries and neuronal precursor cells, a method for the preparation of protein arrays with micron-scale interconnecting tracks for outgrowth guidance is essential. Interconnected patterns can been obtained by thin film PDMS microcontact printing on PLL-coated substrates and used for establishing primary neuronal networks (shown in ESI Fig. 1). However, the replication of micron-scale tracks was insufficiently precise for the reproducible formation of neuronal networks.

In this paper we present an original micron-scale network patterning technique which leverages the protein rejecting qualities of PEG adlayers with the elastomeric feature of soft lithography for rapid replication outside the clean room. Arrays with interconnecting track features for protein adsorption patterning were fabricated by plasma masking PEG adlayers using a bilayer membrane comprising multiple through-holes interfaced with microchannels. This precise and reproducible protein network patterning technique was used to determine optimal dimensions for the formation of high fidelity neuronal networks. These were used to measure the neurodegenerative effects of acrylamide as well as the buffering effects of calpeptin and brain-derived neurotrophic factor (BDNF) during co-treatment.

Materials and methods

Surface PEGylation

Ethanol and plasma cleaned glass substrates were PEGylated with the cationic copolymer of poly-L-lysine grafted with poly(ethylene glycol) by submersion in a 10 mM HEPES (4-(2-hydroxyethyl)-1-piperazine ethanesulfonic acid, pH 7.4) buffer containing 100 μg mL^{-1} of PLL(20)-*g*[3.5]-PEG(2) (Surface Solutions, Switzerland) for 1 h at room temperature. Substrates were then rinsed with a sequence of 1 × phosphate buffered saline (PBS), MilliQ water and a N_2 stream.

Membrane fabrication and plasma masking

To prepare the PDMS membranes a bilayer SU-8 master was fabricated. A first layer of SU-8 2 (Shipley) was spin coated to a depth of ~1.0 μm and patterned using standard photolithography to realise arrays with interconnecting tracks. A second layer of SU-8 50 (Shipley) was spin coated to a depth of ~60 μm, and patterned only as an array of nodes which were aligned to those of the first layer. The resulting hexagonal arrays contained 70-μm-diameter pillars connected *via* microchannels with a length of 100 μm and with widths ranging from 1.0 to 4.0 μm. Arrays containing 367 or 202 nodes were replicated (16 or 36, respectively) across a 24 × 24 mm area. For moulding, a PDMS pre-polymer and curing agent mixture (10 : 1 (wt/wt), Elastosil® RT 601, Wacker) was first degassed and then diluted in silicone fluid (1 : 4 (wt/wt), AK35, Wacker). A 2 mL volume was spin coated at 1600 rpm for 50 s followed by thermal curing at 70 °C for 10 min to produce a ~50-μm-thick coating. To release the delicate PDMS membrane from the SU-8 master and provide a handle for manipulation a thick (≥2 mm) PDMS frame was attached by oxygen plasma bonding (Femto, Diener Electronic) or by applying small quantities of PDMS to act as an adhesive. The bilayer membrane features were imaged using a SEM (Quanta 200F, FEI) and are shown in Fig. 1. Plasma masking involved contacting the bilayer PDMS membranes to the PEGylated substrates followed by plasma etching (70 W, 40 kHz (Femto, Diener Electronic)) in a 0.2 mbar oxygen atmosphere for 60 s.

Surface analysis

Contact angle measurements using a 1 μL sessile water droplet were used to screen the physicochemical properties of the PEGylated surfaces. Zeta potential responses to the addition of bovine serum albumin (Sigma Aldrich, Germany) in a 1 × PBS (pH 7.0) buffer at concentrations ranging from 6 nM to 18 μM

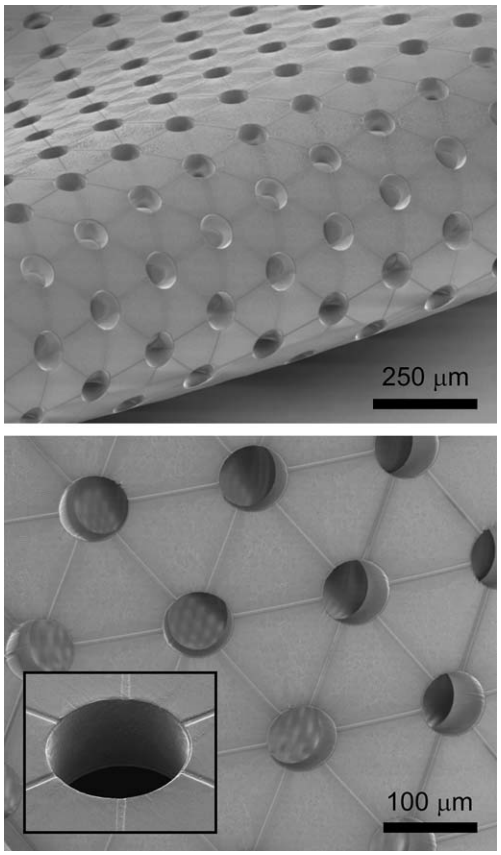

Fig. 1 SEM images of a 50-μm-thick PDMS stencil. The through-holes have a diameter of 70 μm and are interconnected by 100-μm-long microchannels with a height of 1.0 μm and a width of 3.0 μm. The curvature demonstrates the elastomeric quality of the stencil, a feature necessary for conformal contact.

were measured using a SurPASS instrument (Anton Paar, Austria). PLL-*g*-PEG adlayers with and without plasma treatment were compared to plasma treated glass surfaces. The chemical stoichiometry of the PLL-*g*-PEG adlayer before and after oxygen plasma treatment was investigated using X-ray photoelectron spectroscopy (XPS, AXIS-HS-spectrometer Kratos, Manchester, UK). Glass was replaced with silicon substrates with the native oxide providing a glass-like substitute. For excitation a non-monochromatic Mg-Kα radiation source was used, with detection using a hemispherical analyzer with fixed analyzer transmission. Scan surveys were first undertaken using an 80 eV pass energy with 1 eV steps, followed by scans of the O1s, C1s, N1s and Si2p regions using a 20 eV pass energy with 0.1 eV steps. Relative quantification factors were obtained by calibration using poly(ethylene glycol) and poly(sodium 4-styrenesulfonate) standards.

Cell culture and network analysis

The human neuroblastoma cell line SH-SY5Y (DSMZ, Germany) was used in this study and cultured in Dulbecco's modified Eagle medium (DMEM) supplemented with 10% (v/v) foetal bovine serum (FBS), and 1% (v/v) penicillin and streptomycin. Differentiation was achieved by the addition of 10 μM *trans* retinoic acid (Sigma-Aldrich) for 4 days. This also reduces the clustering behaviour, promoting higher levels of array occupancy than a 3 day treatment.[7] Cells were then harvested using 0.25% (w/v) trypsin, seeded on the arrays in a 1 mL suspension containing 2.5×10^5 cells and incubated overnight at 37 °C in a 5% CO_2 atmosphere. The culture medium was then removed and replaced with fresh media also containing retinoic acid. In the process non-adherent cells were removed to reveal the neuronal arrays. A phase contrast inverted microscope (IX71, Olympus) was used to image FITC-labelled protein and cell patterns.

Preliminary experiments used 24 × 24 mm substrates patterned with 16 arrays, each containing 367 nodes. Subsequent experiments used substrates patterned with 36 arrays, each containing 202 nodes. In the majority of the experiments the neuronal networks were assessed in terms of node occupancy, the number of internodal connections and track occupancy. Node occupancy was defined as the percentage of nodes occupied by one or more neurons. The internodal connection measure was defined as the number of neurite interconnections relative to the number of occupied nodes across the entire 202-node array and presented as connections per node (cpn). Track occupancy was defined as the percentage of tracks occupied by one or more neurons. Reproducibility analysis also involved measuring the patterning efficiency.[22] Patterning efficiency E_{patt} was defined as the number of cells adhering to the plasma activated area N_p relative to the number of cells adhering to an equivalent sized, untreated area N_u and was calculated as a percentage according to:

$$E_{patt} = 2 \times \left(\frac{N_p}{N_p + N_u} - \frac{1}{2} \right) \times 100 \quad (1)$$

Acrylamide-induced network degeneration was investigated along with the protective effects of calpeptin and brain derived neurotrophic factor (BDNF). SH-SY5Y cells were differentiated for 4 days using 10 μM *trans* retinoic acid in DMEM containing 10% FBS, and then cultured on the arrays for a further 2 days to establish highly connected neuronal networks. The media was then replaced with serum-free media (B-27®, Invitrogen, Germany) containing retinoic acid and the neuronal networks were treated with 0.5 mM or 1 mM concentrations of the neurotoxin acrylamide (ACR, Sigma-Aldrich, Germany). Cultures were also co-treated daily with 1 μM calpeptin (CP, Merck, Germany) or co-treated once with 100 ng mL^{-1} BDNF (PAN-Biotech, Germany), with the exception of neuronal networks treated only with acrylamide and untreated controls. The integrity of the neuronal networks was measured by scoring neurite connections daily for 3 days. Treatments were undertaken in triplicate. Results were analysed using a 2-factorial 4 × 7 ANOVA using the repeated measurement factor *time* (4-ary: 0, 24, 48 and 72 h after treatment) and the between subject factor *treatment* (7-ary: control, 0.5 mM ACR, 1 mM ACR, 0.5 mM ACR + 1 μM CP, 1 mM ACR + 1 μM CP, 0.5 mM ACR + 100 ng mL^{-1} BDNF, 1 mM ACR + 100 ng mL^{-1} BDNF). The network quality indicator 'connections per node' (cpn) was used as the dependent variable. Dunnett t-tests were used to compare the mean values at the 4 experimental intervals. To simplify the presentation of the results the cpn values were normalized to the respective control conditions. However, all statistical analyses used the raw data.

Results and discussion

Surface chemistry

The electrostatic assembly of the PLL-*g*-PEG adlayer onto the glass substrates[41] reliably produced surfaces which were highly resistant to protein adsorption and cell adhesion,[42] a quality likely resulting from the highly solvated state of the ether (C–O–C) repeats within the brush-like polymer.[43] A coating of PLL (20)-*g*[3.5]-PEG(2) was chosen for minimal protein adsorption (<2 ng cm^{-2}).[44] Zeta potential measurements were used to assess the PLL-*g*-PEG adlayer. Surface coating was rapid, with the zeta potential rising from approximately −120 mV to −40 mV within minutes. XPS analysis also showed that the presence of the PEG adlayer screens the silicon, causing a >10% reduction in the Si2p signal (see Table 1). To confirm the protein rejecting capacity of the adlayer, the zeta potential was measured and remained stable during the stepwise addition of albumin concentrations up to 18 μM (1.20 mg mL^{-1}, see Fig. 2). This result further demonstrates the inert, anti-fouling nature of the PLL-*g*-PEG adlayer.

The effect of plasma treatment on the atomic stoichiometry of the PEGylated surface was assessed by XPS, with results documented in Table 1. The main C1s (*e.g.* C–O–C) and N1s signals from the PLL-*g*-PEG adlayer were markedly diminished while the COOH signal at ~289 eV increased 7-fold. Coupled with the restoration of the Si2p signals, the data indicates that the adlayer had been oxidatively disintegrated. Similar chemical transformations have been observed for the oxidation of PEGylated surfaces by UV irradiation.[39,40] The water contact angle of the PEGylated surfaces was reduced from 29.1° (SD ± 2.1°) to <5°, a value consistent with oxygen plasma treated glass substrates. Indeed, the zeta potential responses of the plasma treated PLL-*g*-PEG adlayer and the plasma treated glass substrate to additions of albumin were nearly identical (see Fig. 2). Here, the zeta potential increased from −125 mV to −73 mV during the addition of albumin to a final concentration of 18 μM. Together these results indicate that plasma treatment disintegrates the PLL-*g*-PEG adlayer to produce a glassy-like surface suitable for protein adsorption.

Protein and neuronal network patterning

PDMS membranes with through-holes have previously been used for surface[46] and cell patterning.[47–49] A drawback is the requirement for the membrane to be self-supporting which prevents the inclusion of continuous and interconnected patterns within the membrane. In addition, the limited aspect ratio of the mould coupled with the fragility of thin (<10 μm) PDMS membranes also prevents the inclusion of micron-sized features. To overcome these limitations we have developed a bilayer membrane masking approach, which combines through-hole features with microchannels for the production of micron-scale interconnecting patterns by masked oxygen plasma treatment.

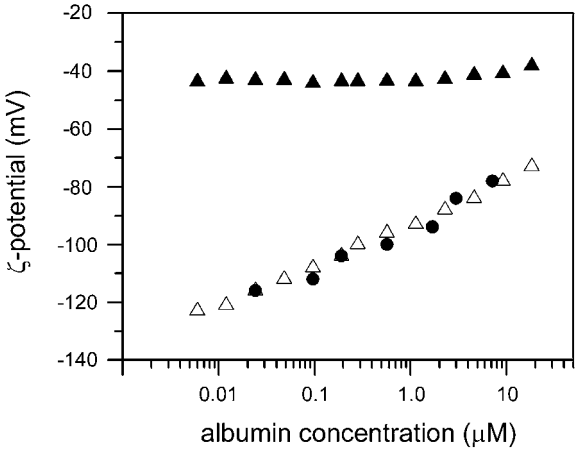

Fig. 2 Zeta potential measurement of glass (black points), PLL-*g*-PEG (black triangles) and plasma treated PLL-*g*-PEG (white triangles) recorded during the stepwise addition of 6 nM to 18 μM concentrations of albumin.

Plasma masking was simple and rapid, reliably replicating the stencil features across the entire masked area. An oxygen plasma treatment for 12 s produced oxidation patterns in the PEG adlayer with even the smallest channel features (1-μm-wide). The oxygen plasma could therefore penetrate 100-μm-long channels with a cross sectional area of 1 μm^2 in a matter of seconds. The selective adsorption of FITC-conjugated proteins was used to image the oxidation patterns. As shown in Fig. 3(A) and ESI Fig. 2, high resolution (SD ± 220 nm) micron-scale oxidation patterns were faithfully transferred to the PEGylated surface. Micron-scale resolution patterning of protein-rejecting surface coatings can also be achieved using scanning laser ablation techniques.[10,50] Such techniques offer greater freedom of design and, in a stepwise fashion, can be used to pattern multiple proteins.[50] For the fabrication of smaller, nanoscale patterns scanning near-field optical microscopy (SNOM) methods can be used,[51] although as with other scanning methods fabrication becomes time consuming.

Table 1 XPS atomic percentage data from the PLL-*g*-PEG adlayer with and without 60 s oxygen plasma treatment

electron level:	O1s (at. %)	C1s 1 (at. %)	C1s 2 (at. %)	C1s 3 (at. %)	C1s 4 (at. %)	N1s (at. %)	Si2p 1 (at. %)	Si2p 2 (at. %)
probable species:[45]	all	C–C, C–H	C–O–C, C–OH, C–N, C–NH_3^+, C=N, C≡N	C=O, O–C–O, N–C–O, N–C≡O	COOH, N–(C=O)O	N–C, N≡C, N–C=O, N–(C=O)O, NH_3^+, $N(CH_3)_3^+$	Si^0	SiO_2
sample								
native Si	35.56	2.04	0.45	0.89	0.82	0.53	47.65	12.06
PEGylated Si	33.52	2.77	12.72	1.64	0.26	1.45	39.23	8.88
Plasma treated PEGylated Si	34.80	0.92	0.18	0.21	1.78	0.53	48.25	13.33

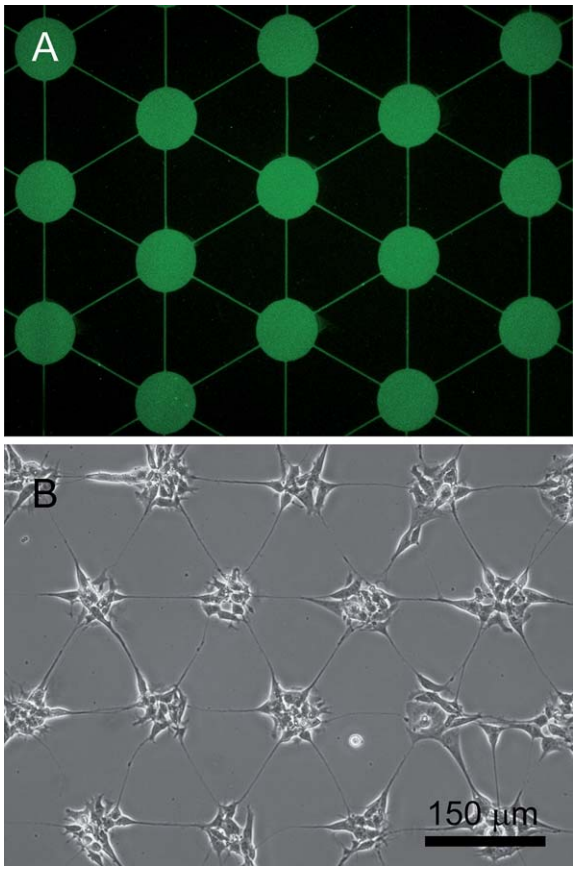

Fig. 3 High fidelity protein patterning and network formation. The selective assembly of FITC-conjugated proteins on the plasma-oxidised regions demonstrates the precision patterning capability (A). Differentiated SH-SY5Y neurons were confined to the array nodes with neurite outgrowth guidance resulting in the formation of internodal connections (B).

It is the elastomeric nature of the PDMS material which ensures conformal contact for such precision feature replication outside the clean room. In comparison, protein patterning by μCP, another soft lithography technique, cannot rival the across pattern reproducibility and with micron features separated by 100 μm distances the elastomeric stamp frequently collapses for the unwanted transfer of proteins.[16,32,52,53] This drawback is bypassed when using membranes which have an inverted relief structure to those required for μCP. The microchannels within the bilayer membrane are reminiscent of those used for material patterning by micromolding in capillaries (MIMIC).[26] However, the dense array of small through-holes in the bilayer membrane are not suitable for defining inlet to outlet flow paths necessary for the controlled distribution of liquid throughout the entire network.

The plasma masking technique also has good throughput. The plasma chamber can accommodate multiple substrates, patterning is rapid and the membranes are reusable (x40). Together these attributes make the technique highly convenient for meeting the replicate demands of typical neurobiology experiments. The plasma oxidized surface patterns were subsequently tested for their suitability for arraying human SH-SY5Y neurons and for guiding neurite outgrowths to interconnect the cellular nodes. Here, conformationally intact adhesion proteins from the culture media selectively assemble on the oxidized regions and act to direct the formation of a neuronal network. The masked PEGylated surfaces retained their ability to resist cell adhesion, resulting in high pattern compliance. An entire 367-node array with 97% of the nodes occupied and a >99% patterning efficiency is shown in ESI Fig. 3. Without track features network formation was limited to 0.012 connections per node (cpn) by the fourth day, demonstrating that, unlike thin film PDMS patterns (0.88 cpn),[7] the PEGylated surfaces strongly resist the locomotion of growth cones and the extension of neurite outgrowths. A preliminary screen of different node diameters and different connection distances was undertaken. Arrays containing 70-μm-diameter nodes were optimal for high occupancy levels (>90%) and high patterning efficiency (>99%), while a track length of 100 μm was optimal for the development of high neurite interconnection levels. An image of a neuronal network developed during a 3 day culture period is shown in Fig. 3(B), with a larger area (~2 mm^2) of the network documented in ESI Fig. 4.

Network plasticity

Neuronal networks located within an array format are straightforward to visualize, negating the need for fixation and staining which enables network dynamics to be periodically or continuously recorded. Neuronal network development on a 0.55 mm^2 region of an array with 4-μm-wide tracks was recorded using time lapse video microscopy (see ESI video link). Throughout the 5 day development phase the network was highly dynamic, with interconnections being formed, being retracted and being re-established, before finally leading to 1.0 cpn. Network development is plotted in ESI Fig. 5 and, although positional information is not captured, illustrates the plasticity occurring within the dynamics of the network formation process. The video also documents high levels of neuronal migration between nodes, a quality assisted by the generous 4-μm-wide tracks. However, such levels of migration limit the ability to score neurite interconnections with a defined length of 100 μm.

Optimum track width for neurite outgrowth

A systematic study of the optimum track width required for the development of highly connected neuronal networks has not been previously reported. The precision network patterning capability afforded by the bilayer membrane plasma masking technique makes this possible. Shown in ESI Figs. 5 and 6, and also illustrated in the ESI video, a track width of 4 μm was excessive, with large numbers of neurons migrating between nodes by adhesive locomotion along the track features. The adhesion of neurons on the track features is especially undesirable for the network formation assay (NFA) as this voids neurite outgrowth length standardization, a pre-requisite for neurite counting.[7,54] Track widths ranging from 1.0 μm to 3.0 μm were evaluated for optimal network formation levels, with results documented in Fig. 4(A). Neurite outgrowth and network formation was sensitive to track width differences as small as 500 nm. The rate of network formation increased with track width. With the use of 1-μm-wide tracks network formation levels

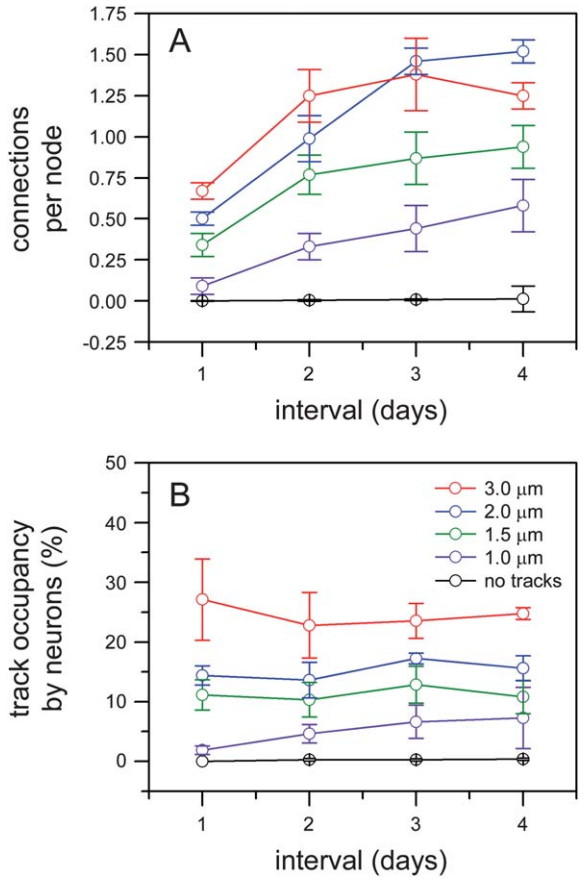

Fig. 4 Network development was sensitive to the width of the micron-scale tracks (A). Neuronal occupancy of the track features increased with track width (B).

reached 0.58 cpn (SD ± 0.16) during a 4 day development period, whereas with the use of 2.0-µm-wide tracks levels were increased to 1.52 cpn (SD ± 0.07). However, with the largest 3.0-µm-wide tracks neuronal networks attained plateau levels by the second day, with a maximum value of only 1.38 cpn (SD ± 0.22) on the third day. These tracks were significantly occupied (~25%) by neurons, prohibiting the scoring of complete neurite outgrowth connections. Shown in Fig. 4(B), the width also correlated with neuron occupancy of the tracks with levels being relatively stable throughout the duration of culture (for widths >1 µm). Taken together, the results demonstrate that a track width of 2.0 µm is optimal for high network formation levels and low track occupancy (~15%). Arrays containing 70-µm-diameter nodes separated by 100-µm-long tracks with a 2.0 µm width were used for subsequent experiments.

Network patterning reproducibility

Reproducible cell patterning is a pre-requisite for spatially standardized cell assays such as the NFA. The reproducibility of neuronal arraying and network formation on the patterns prepared by plasma masking with a bilayer membrane was assessed on the second day of culture in an experiment involving 3 batches, each containing 3 microchips. The across chip (involving 9 arrays, each containing 202 nodes), chip-to-chip and batch-to-batch reproducibility was excellent. Array occupancy levels were consistent at 95.0% (SD ± 0.6%) and, combined with the cell adhesion resistant quality of the PEG adlayer, led to patterning efficiencies >99.5%. Network formation levels were 0.91 cpn (SD ± 0.10). The variance in the neurite connection levels is presented as a box and whiskers plot in Fig. 5. Within each batch the chip-to-chip coefficient of variation (CV) was 7.25%, with a batch-to-batch CV of 5.95%. This variance could be attributed to the plasticity within the network formation process (see ESI Fig. 5), the different passage numbers (9–12) and the inherent variability of the neurite outgrowth process. Nevertheless, this data reflects the reliability of the bilayer membrane plasma masking technique, the reproducibility of arraying differentiated SH-SY5Y cells and directing network formation at consistent levels.

The network formation assay and connection scoring

The extreme precision and reproducibility of the bilayer membrane plasma masking technique makes it ideally suited for undertaking the network formation assay (NFA).[7,8] The assay measures neurite outgrowth, a hallmark neurodevelopmental indicator, by quantifying internodal connection levels. The hexagonal array format contains uniformly spaced neuronal adhesion sites to standardize the neurite outgrowth length and thereby eliminate length measurements which are otherwise required to satisfy the morphological neurite classification criteria.[7,54] Nodes in the array were separated by 100 µm, a distance also sufficient for the differentiation of neurites into axons with functional synapses.[55,56] Multiple connections can be formed between nodes, with the *pioneer* neurite connection often becoming suspended (see ESI Fig. 7(A)), thereby vacating the track for outgrowth by another neurite (see ESI Fig. 7(B)). To avoid difficulties discerning the number of connections shared between a pair of nodes we chose to score multiple connections as a single connection.

Analysis of network degeneration and protection processes

We have previously used the NFA to quantify the dose-dependent inhibition of neurite outgrowth by the neurotoxin

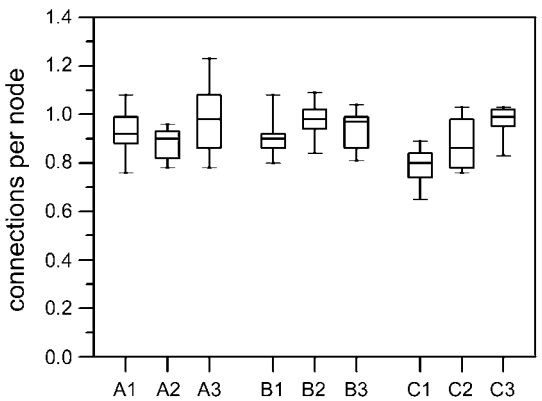

Fig. 5 Network formation reproducibility. The across chip (9 arrays) variation in network formation levels from 3 batches (A–C), each containing 3 chips. The box and whiskers plot presents the mean, the lower 25th and upper 75th percentiles, along with the data extremes.

acrylamide.[7] Acrylamide neurotoxicity in humans is characterized by central-peripheral distal axonopathy with clinical manifestations such as numbness of the hands and feet or altered nerve conduction velocity.[57] *In vitro*, acrylamide can also cause the degeneration of pre-existing neurite outgrowths.[58] Acrylamide's neurotoxic modes of action are various, one of which may be by elevating intracellular Ca^{2+} levels.[58] This causes the Ca^{2+}-dependent up-regulation of calpains, a class of cysteine proteases which degrade neurofilament proteins, spectrin, tubulin and microtubule-associated proteins.[59–61] At physiological levels calpains control, amongst other processes, the mobilization of vesicles to depleted release sites and therefore play a critical role in synaptic facilitation and post-tetanic potentiation.[62] However, with a high Ca^{2+} influx calpain is excessively up-regulated, and causes progressive structural damage to the neuronal cytoskeleton and neuronal networks.[59,61] In contrast, diminished calpain activity is associated with higher neurite outgrowth rates,[61,63] such that the general calpain inhibitor calpeptin can be used to buffer the degenerative effects of acrylamide[58] or elevated Ca^{2+} levels in general.[64]

The interconnected adhesive patterns produced by plasma masking with a bilayer membrane assist the development of high network formation levels which aid the investigation of neurodegenerative processes. In this study we have used the NFA to measure the neurodegenerative effects of 0.5 mM and 1.0 mM concentrations of acrylamide and, by co-treatment, the protective effects of calpeptin (1 μM daily) and brain-derived neurotrophic factor (BDNF, 100 ng mL^{-1}), a protein with wide ranging functions including promoting the differentiation and survival of central nervous system neurons.[65] Differentiated SH-SY5Y cells were cultured on the arrays for 2 days to establish mature, highly connected (~1.3 cpn) networks. Acrylamide treatment for 3 days caused network degeneration. The time courses of acrylamide-induced network degeneration and the buffering effects of co-treatment with calpeptin and BDNF are presented in Fig. 6 as cpn values normalized to the controls, with the raw data plotted in ESI Fig. 8. ANOVA analysis revealed a significant time-treatment interaction ($F_{(18.42)} = 2.19$; $p = 0.024$) indicating dose-dependent network degeneration. With 1 mM acrylamide treatments, degeneration was not evident during the first 48 h, but by 72 h network levels were significantly reduced. Co-treatment with calpeptin or BDNF was insufficient to prevent network degeneration.

The post-hoc test showed that 72 h of treatment with 0.5 mM acrylamide was also required before a reduction in the connections per node was evident (mean difference: −0.46 cpn), but with lower significance ($p = 0.095$). At this concentration calpeptin co-treatment buffered the action of acrylamide, with only an 18% mean reduction in network levels compared to 44% without calpeptin. The NFA is a spatial refinement of the neurite outgrowth assay. This traditional assay has previously been used to measure a 52% reduction in outgrowth levels for neurons treated with 0.5 mM acrylamide for 3 days, with calpeptin co-treatment buffering the reduction to 17%.[58] The close similarity between results generated by the different methods underscores the reliability of the NFA, with the NFA aided by gains in analytical throughput.[7] The data similarity also indicates that patterned culture does not perturb neurite outgrowth.

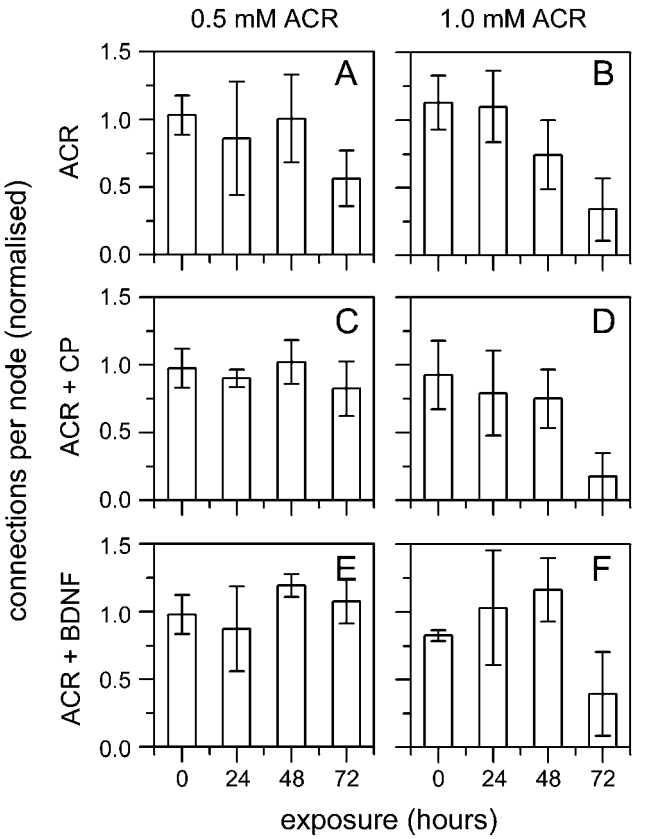

Fig. 6 Dynamics of network degeneration during exposure to 0.5 mM (A) and 1 mM (B) acrylamide concentrations. The buffering effects of 1 μM calpeptin (C,D) and 100 ng mL^{-1} BDNF (E,F) during exposure to 0.5 mM and 1 mM acrylamide, respectively. Network levels were normalized relative to control levels.

Protection with BDNF provided a strong buffering capacity, completely maintaining network integrity. BDNF binds to the tyrosine kinase B (TrkB) receptor and impacts various signaling pathways, including activation of the transcription factor CREB which mediates the expression of genes involved in the molecular processes underlying aspects of memory function.[66] Differentiation of the SH-SY5Y cell line with retinoic acid leads to the expression of TrkB receptors for further differentiation with BDNF to produce cells which exhibit many of the features of mature neurons.[67] Besides the general neuroprotective effect, co-treatment with BDNF will therefore also stimulate pathways required for the fuller maturation of the neuronal networks.[68] In such contexts, the NFA could be used in combination with other analytical tools to draw associations between toxic molecular perturbations and possible neurobehavioural outcomes.

Technical perspectives

A major advantage of the bilayer membrane plasma masking technique is that proteins can be applied by the end-user just prior to experimentation. This feature makes the approach suitable for distributed testing by collaborating groups. In addition to the wider implementation of the assay, high content and high throughput screening PEG arrays can be realised using larger substrates for packaging within industry standard 96-well

and 384-well plates. Shown in ESI Fig. 9, we have adapted a magnetic interfacing technique invented in our laboratory[69,70] for use with a PDMS gasket array to provide a compression seal between a patterned substrate and a bottomless polycarbonate 96-well plate. Automated imaging and analysis will also provide significant gains in throughput,[7,10,71,72] and brings the enticing possibility of obtaining deeper insights into the dynamics of network behaviour.

Conclusions

Plasma masking with a bilayer membrane enables precision oxidative patterning. With optimal dimensions the technique can be used to pattern PEGylated surfaces for the reproducible formation of spatially standardized neuronal networks. These have been used as an analytical platform to measure the time and concentration dependent network degeneration effects caused by the neurotoxin acrylamide and the counteracting effects of calpeptin and BDNF. Beyond these examples, the neuronal networks can be applied to the investigation of a range of structural and kinetic processes in neurobiology.

Acknowledgements

The authors are grateful to Sarah Waide for cell culture support, Silke Kittle for XPS analysis and Maria Becker for SEM imaging. The research was financially supported by the European Community's Seventh Framework Programme (FP7/2007–2013) under grant agreement n° HEALTH-F5-2008-201619 (ESNATS), the German Research Foundation (DFG grant WE3737/3-1), the German Federal Ministry of Education and Research (BMBF grant 0101-31P6541) and the Ministry of Innovation, Science, Research and Technology of the State of North Rhine-Westphalia. Heike Hardelauf thanks the International Leibniz Graduate School "Systems Biology Lab-on-a-Chip" for financial support.

References

1 M. Théry, *J. Cell Sci.*, 2010, **123**, 4201–4213.
2 C. M. Nelson and J. Tien, *Curr. Opin. Biotechnol.*, 2006, **17**, 518–523.
3 D. Castel, A. Pitaval, M.-A. Debily and X. Gidrol, *Drug Discovery Today*, 2006, **11**(13–14), 616–622.
4 S. R. Khetani and S. N. Bhatia, *Nat. Biotechnol.*, 2008, **26**(1), 120–126.
5 F. Hirschhaeuser, H. Menne, C. Dittfeld, J. West, W. Mueller-Klieser and L. A. Kunz-Schughart, *J. Biotechnol.*, 2010, **148**(1), 3–15.
6 H. Hardelauf, J.-P. Frimat, J. D. Stewart, W. Schormann, Y.-Y. Chiang, P. Lampen, J. Franzke, J. G. Hengstler, C. Cadenas, L. A. Kunz-Schughart and J. West, *Lab Chip*, 2011, **11**, 419–428.
7 J.-P. Frimat, J. Sisnaiske, S. Subbiah, H. Menne, P. Godoy, P. Lampen, M. Leist, J. Franzke, J. G. Hengstler, C. van Thriel and J. West, *Lab Chip*, 2010, **10**, 701–709.
8 J. West, J.-P. Frimat, J. Sisnaiske, C. van Thriel and J. G. Hengstler, DE 10 2009 021 876.9 and PCT/EP2010/002811.
9 K. Schauer, T. Duong, K. Bleakley, S. Bardin, M. Bornens and B. Goud, *Nat. Methods*, 2010, **7**(7), 560–568.
10 Z. D. Wissner-Gross, M. A. Scott, D. Ku, P. Ramaswamy and M. F. Yanik, *Int. Bio.*, 2011, **3**, 65–74.
11 D. Kleinfeld, K. H. Kahler and P. E. Hockberger, *J. Neurosci.*, 1988, **8** (11), 4098–4120.
12 S. Rohr and B. M. Salzberg, *Biophys. J.*, 1994, **67**, 1301–1315.
13 E. V. Romanova, K. A. Fosser, S. S. Rubakhin, R. G. Nuzzo and J. V. Sweedler, *FASEB J.*, 2004, **18**(11), 1267–1269.
14 Y. Mourzina, D. Kaliaguine, P. Schulte and A. Offenhäusser, *Anal. Chim. Acta*, 2006, **575**, 281–289.
15 F. Patolsky, B. P. Timko, G. Yu, Y. Fang, A. B. Greytak, G. Zheng and C. M. Lieber, *Science*, 2006, **313**, 1100–1104.
16 S. B. Jun, M. R. Hynd, N. Dowell-Mesfin, K. L. Smith, J. N. Turner, W. Shain and S. J. Kim, *J. Neurosci. Methods*, 2007, **160**, 317–326.
17 M. S. Ravenscroft, K. E. Bateman, K. M. Shaffer, H. M. Schessler, D. R. Jung, T. W. Schneider, C. B. Montgomery, T. L. Custer, A. E. Schaffner, Q. Y. Liu, Y. X. Li, J. L. Barker and J. J. Hickman, *J. Am. Chem. Soc.*, 1998, **120**(47), 12169–12177.
18 A. Welle, S. Horn, J. Schimmelpfeng and D. Kalka, *J. Neurosci. Methods*, 2005, **142**, 243–250.
19 J. M. Corey, B. C. Wheeler and G. J. Brewer, *IEEE Trans. Biomed. Eng.*, 1996, **43**(9), 944–955.
20 E. Detrait, J.-B. Lhoest, B. Knoops, P. Bertrand and P. van den Bosch de Aguilar, *J. Neurosci. Methods*, 1998, **84**, 193–204.
21 S. W. Rhee, A. M. Taylor, C. H. Tu, D. H. Cribbs, C. W. Cotman and N. L. Jeon, *Lab Chip*, 2005, **5**, 102–107.
22 J.-P. Frimat, H. Menne, A. Michels, S. Kittel, R. Kettler, S. Borgmann, J. Franzke and J. West, *Anal. Bioanal. Chem.*, 2009, **395**(3), 601–609.
23 K. E. Healy, B. Lom and P. E. Hockberger, *Biotechnol. Bioeng.*, 1994, **43**, 792–800.
24 A. Douvas, P. Argitis, K. Misiakos, D. Dimotikali, P. S. Petrou and S. E. Kakabakos, *Biosens. Bioelectron.*, 2002, **17**, 269–278.
25 H. Sorribas, C. Padesta and L. Tiefenauer, *Biomaterials*, 2002, **23**, 893–900.
26 R. S. Kane, S. Takayama, E. Ostuni, D. E. Ingber and G. M. Whitesides, *Biomaterials*, 1999, **20**, 2363–2376.
27 A. Bernard, E. Delamarche, H. Schmid, B. Michel, H. R. Bosshard and H. Biebuyck, *Langmuir*, 1998, **14**, 2225–2229.
28 Y. Xia and G. M. Whitesides, *Angew. Chem., Int. Ed.*, 1998, **37**, 550–575.
29 G. M. Whitesides, E. Ostuni, S. Takayama, X. Jiang and D. E. Ingber, *Annu. Rev. Biomed. Eng.*, 2001, **3**, 335–373.
30 A. K. Vogt, G. Wrobel, W. Meyer, W. Knoll and A. Offenhäusser, *Biomaterials*, 2005, **26**, 2549–2557.
31 J. Fink, M. Théry, A. Azioune, R. Dupont, F. Chatelain, M. Bornens and M. Piel, *Lab Chip*, 2007, **7**, 672–680.
32 D. Falconnet, A. Koenig, F. Assi and M. Textor, *Adv. Funct. Mater.*, 2004, **14**(8), 749–756.
33 A. Ruiz, L. Buzanska, D. Gilliland, H. Rauscher, L. Sirghi, T. Sobanski, M. Zychowicz, L. Ceriotti, F. Bretagnol, S. Coecke, P. Colpo and F. Rossi, *Biomaterials*, 2008, **29**, 4766–4774.
34 M. Zhang, T. Desai and M. Ferrari, *Biomaterials*, 1998, **19**, 953–960.
35 M. Malmsten, K. Emoto and J. M. van Alstine, *J. Colloid Interface Sci.*, 1998, **202**, 507–517.
36 G. Cuscs, R. Michel, J. W. Lussi, M. Textor and G. Danuser, *Biomaterials*, 2003, **24**, 1713–1720.
37 C. H. Thomas, J.-B. Lhoest, D. G. Castner, C. D. McFarland and K. E. Healy, *J. Biomech. Eng.*, 1999, **121**, 40–47.
38 S. S. Shah, M. C. Howland, L.-J. Chen, J. Silangcruz, S. V. Verkhoturov, E. A. Schweikert, A. N. Parikh and A. Revzin, *ACS Appl. Mater. Interfaces*, 2009, **1**(11), 2592–2601.
39 A. Azioune, M. Storch, M. Bornens, M. Théry and M. Piel, *Lab Chip*, 2009, **9**, 1640–1642.
40 S. A. Ahmad, A. Hucknall, A. Chilkoti and G. J. Leggett, *Langmuir*, 2010, **26**(12), 9937–9942.
41 G. L. Kenausis, J. Vörös, D. L. Elbert, N. Huang, R. Hofer, L. Ruiz-Taylor, M. Textor, J. A. Hubbell and N. D. Spencer, *J. Phys. Chem. B*, 2000, **104**, 3298–3309.
42 N.-P. Huang, R. Michel, J. Vörös, M. Textor, R. Hofer, A. Rossi, D. L. Elbert, J. A. Hubbell and N. D. Spencer, *Langmuir*, 2001, **17**, 489–498.
43 P. Roach, T. Parker, N. Gadegaard and M. R. Alexander, *Surf. Sci. Rep.*, 2010, **65**, 145–173.
44 S. Pasche, S. M. De Paul, J. Vörös, N. D. Spencer and M. Textor, *Langmuir*, 2003, **19**, 9216–9225.
45 G. Beamson and D. Briggs, In *High resolution XPS of organic polymers: The Scienta ESCA 300 Database*. Wiley, Chichester, 1992.
46 R. J. Jackman, D. C. Duffy, O. Cherniavskaya and G. M. Whitesides, *Langmuir*, 1999, **15**, 2973–2984.
47 A. Folch, B.-H. Jo, O. Hurtado, D. J. Beebe and M. Toner, *J. Biomed. Mater. Res.*, 2000, **52**, 346–353.
48 E. Ostuni, R. Kane, C. S. Chen, D. E. Ingber and G. M. Whitesides, *Langmuir*, 2000, **16**, 7811–7819.

49 A. Tourovskaia, T. Barber, B. T. Wickes, D. Hirdes, B. Grin, D. G. Castner, K. E. Healy and A. Folch, *Langmuir*, 2003, **19**, 4754–4764.
50 A. D. Doyle, F. W. Wang, K. Matsumoto and K. M. Yamada, *J. Cell Biol.*, 2009, **184**(4), 481–490.
51 S. A. Ahmad, A. Hucknall, A. Chilkoti and G. J. Legget, *Langmuir*, 2010, **26**(12), 9937–9942.
52 Y. Xia and G. M. Whitesides, *Annu. Rev. Mater. Sci.*, 1998, **28**, 153–184.
53 D. Falconnet, G. Csucs, H. M. Grandin and M. Textor, *Biomaterials*, 2006, **27**, 3044–3063.
54 N. M. Radio and W. R. Mundy, *NeuroToxicology*, 2008, **29**, 361–375.
55 C. G. Dotti, C. A. Sullivan and G. A. Banker, *J. Neurosci.*, 1988, **8**(4), 1454–1468.
56 D. A. Stenger, J. J. Hickman, K. E. Bateman, M. S. Ravenscroft, W. Ma, J. J. Pancrazio, K. Shaffer, A. E. Schaffner, D. H. Cribbs and C. W. Cotman, *J. Neurosci. Methods*, 1998, **82**, 167–173.
57 C. J. Calleman, Y. Wu, F. He, G. Tian, E. Bergmark, S. Zhang, H. Deng, Y. Wang, K. M. Crofton, T. Fennell and L. G. Costa, *Toxicol. Appl. Pharmacol.*, 1994, **126**(2), 361–371.
58 M. Nordin-Andersson, E. Walum, P. Kjellstrand and A. Forsby, *Cell Biol. Toxicol.*, 2003, **19**, 43–51.
59 D.-K. Song, T. Malmstrom, S. B. Kater and D. L. Mykles, *J. Neurosci. Res.*, 1994, **39**, 474–481.
60 D. E. Goll, V. F. Thompson, H. Li, W. Wei and J. Cong, *Physiol. Rev.*, 2003, **83**, 731–801.
61 V. Axelsson, S. Holback, M. Sjögren, H. Gustafsson and A. Forsby, *Biochem. Biophys. Res. Commun.*, 2006, **345**, 1068–1074.
62 A. Khoutorsky and M. E. Spira, *Learn. Mem.*, 2009, **16**, 129–141.
63 M. Oshima, S. Koizumi, K. Fujita and G. Guroff, *J. Biol. Chem.*, 1989, **264**(34), 20811–20816.
64 A. Das, D. P. Garner, A. M. Del Re, J. J. Woodward, D. M. Kumar, N. Agarwal, N. L. Banik and S. K. Ray, *Brain Res.*, 2006, **1084**, 146–157.
65 C. Cunha, R. Brambilla and K. L. Thomas, *Front. Mol. Neurosci.*, 2010, **3**, 1–14.
66 E. R. Kandel, *J. Neurosci.*, 2009, **29**(41), 12748–12756.
67 L. Agholme, T. Lindström, K. Kågedal, J. Marcusson and M. Hallbeck, *J. Alzheimers Dis.*, 2010, **20**, 1069–1082.
68 T.-J. Chen, H.-M. Cheng, D.-C. Wang and H.-S. Hung, *Toxicol. Lett.*, 2011, **200**, 67–76.
69 J. Franzke, P. Jacob and J. West, DE 10 2007 037 788.8.
70 J. Atencia, G. A. Cooksey, A. Jahn, J. M. Zook, W. N. Vreeland and L. E. Locascio, *Lab Chip*, 2010, **10**, 246–249.
71 R. D. Price, T. Oe, T. Yamaji and N. Matsuoka, *J. Biomol. Screening*, 2006, **11**(2), 155–164.
72 N. M. Radio, J. M. Breier, T. J. Shafer and W. R. Mundy, *Toxicol. Sci.*, 2008, **105**(1), 106–118.